

Simulation of a Standing Passenger during Driveaway using Optimal Control

Monika Harant¹, Marius Obentheuer¹, Michael Roller¹, Joachim Linn¹

¹ Mathematics for the Digital Factory
Fraunhofer Intitute for Industrial Mathematics
Fraunhofer-Platz 1, 67663 Kaiserslautern, Germany
{monika.harant, marius.obentheuer, michael.roller, joachim.linn}@itwm.fraunhofer.de

ABSTRACT

Digital Human models play an important part in vehicle development and safety studies. Currently, they are mainly used in static ergonomics studies or highly dynamic and complex crash simulations. In this work, we present the use of human models for scenarios that lie between these domains. Using optimal control, we simulate the dynamic behavior of a passenger during a bus driveaway. The human is modeled as a rigid multibody system transferred of the 50th percentile male of the THUMS 'family' and is actuated via different actuation models. Using discrete mechanics and optimal control for constrained systems (DMOCC), the actuation profiles are optimized for different scenarios and motion strategies and then compared. The simulation results show that the compensation of the starting maneuver is significantly more difficult with an orientation against the driving direction in contrast to an orientation in the driving direction.

Keywords: Optimal Control, Biomechanics, Human Modeling, Multibody Dynamics, Vehicle Ergonomics.

1 INTRODUCTION

As computing power increases and digital human models (DHM) continue to evolve, they are increasingly being used for investigations in vehicle development and safety, e.g., in [1, 2]. While in the past mainly crashes and driver ergonomics were investigated, now also passengers of buses and trains are more in the focus of vehicle ergonomics and safety studies, as in [2, 3]. Their investigation is more complex, since many more posture and movement variations must be considered. FEM models [4, 5] that are commonly used for crash simulations are currently not able to cover all interesting scenarios in this field, since the actuation capabilities of these models are still very limited and so far can be used mainly to maintain a given initial position. DHM for ergonomics studies [3, 6] are used for decades to ensure a comfortable usage of the vehicles but they mostly allow only posture or quasistatic movement evaluation, i.e., the movement is approximated by a series of postures and no velocities or acceleration are considered in the dynamics calculations. This is however required when wanting to investigate passenger movements during highly dynamic driving maneuvers, e.g. the accelerations imposed on the passenger during the driveaway of a bus.

Optimal control of multibody systems enables simulation of active motions and has been successfully applied to various sports, lifting motions, or motions using prostheses [7, 8, 9]. It optimizes control patterns, in the case of DHM, joint moments or muscle activation that minimize certain optimality criteria while satisfying the system's equation of motion and various constraints. These optimality criteria are combined into an objective function and determine the characteristics of the motion. This is based on the assumption that human motion is optimally controlled, whether in a time- or energy-efficient manner or with respect to more task-specific goals. This makes it a promising tool to simulate and analyze the motion and comfort of vehicle occupants during different driving maneuvers.

In this work, which is part of the project "EMMA4Drive", we apply optimal control to simulate and analyze the occupant behavior in a departing bus. The passenger is modeled as a rigid multibody system, which is actuated by different actuation models: muscle models, muscle torque generators (MTG), and motors. The kinematic structure and dynamic properties were transferred from the 50 percentile male of the THUMS 'family' [4]. Several multiphase optimal control problems (OCP) were set up, solved, and evaluated that simulate the driveaway of the bus, included a phase that models the response time of the passenger to the sudden perturbation. First, we describe the modeling of the different components of the passenger and the OCPs in Section 2. Then we present the simulation results (Section 3) and conclude with a discussion of the methodology and results (Section 4).

2 Methods

This section introduces different modeling aspects of the passenger and driveaway simulation. These include modeling the bus and the passenger as rigid (multi)body systems (RMBS) (Section 2.1), the actuation of the human (Section 2.2), and the contacts between the passenger and the bus (Section 2.3). We then describe the optimal control problems with their phase division and the objective functions considered (Section 2.4).

2.1 Model Creation of Passenger and Bus

The bus consists of a movable platform with one translatory degree of freedom in the direction of driving. A vertical hand rail is rigidly coupled on top at the side of the platform. The passenger is modeled as RMBS with 40 degrees of freedom, of which 34 are actuated. The finite-element model of a 50th percentile male (height 1.78 m, weight 77.1 kg) of the THUMS 'family' was used as a basis and transferred to a RMBS using the kinematic structure proposed by [10]. The bones of the THUMS model were exported to stl-files. Certain locations in the structure (ankle, knee, hip joint, L5/S1 joint, T1/C7 joint, shoulder, elbow, and wrist) were made movable by appropriate joints so that the model is able to reproduce the range of motion of a human being. Fingers and toes were not made movable. Mass, the center of mass (CoM) location, and inertia of the individual segments of the human were also transferred from the THUMS model. For this purpose, the values of each finite element part of the FEM model in default posture were determined (see Figure 1), 1292 parts in total. Each part was manually assigned to a link in the RMBS based on its location and its values were transferred to the coordinate system of the link. For each part, a rigid body was defined using the part's mass, CoM, and inertia and all parts assigned to a segment were merged so that one body was obtained with the combined masses, center of masses and inertia tensors with the following procedure. Two rigid bodies B_1 and B_2 with respective masses M_{B_1} and M_{B_2} , CoMs \mathbf{c}_{B_1} and \mathbf{c}_{B_2} , and inertia \mathbf{I}_{B_1} and \mathbf{I}_{B_2} can be merged to one body B with mass M , CoM \mathbf{c} , and inertia \mathbf{I} by

$$M = M_{B_1} + M_{B_2}, \quad (1)$$

$$\hat{\mathbf{c}}_{B_2} = \mathbf{R}_{B_1}^{B_2 T} \mathbf{c}_{B_2} + \mathbf{r}_{B_1 B_2}^{\rightarrow}, \quad (2)$$

$$\mathbf{c} = \frac{1}{M} (M_{B_1} \mathbf{c}_{B_1} + M_{B_2} \hat{\mathbf{c}}_{B_2}), \quad (3)$$

$$\hat{\mathbf{I}}_{B_2} = \mathbf{R}_{B_1}^{B_2 T} (\mathbf{I}_{B_2} - M_{B_2} [\mathbf{c}_{B_2}]_{\times} [\mathbf{c}_{B_2}]_{\times}^T) \mathbf{R}_{B_1}^{B_2} + M_{B_2} [\hat{\mathbf{c}}_{B_2}]_{\times} [\hat{\mathbf{c}}_{B_2}]_{\times}^T, \quad (4)$$

$$\mathbf{I} = \mathbf{I}_{B_1} + \hat{\mathbf{I}}_{B_2} - M [\mathbf{c}]_{\times} [\mathbf{c}]_{\times}^T, \quad (5)$$

with $\mathbf{R}_{B_1}^{B_2} \in \mathbf{SO}(3)$ and $\mathbf{r}_{B_1 B_2}^{\rightarrow} \in \mathbb{R}^3$ describing the transformation from the frame of B_1 to the frame of B_2 . The CoM and the inertia of B_2 with respect to the frame of B_1 is denoted by $\hat{\mathbf{c}}_{B_2}$ and $\hat{\mathbf{I}}_{B_2}$, respectively.

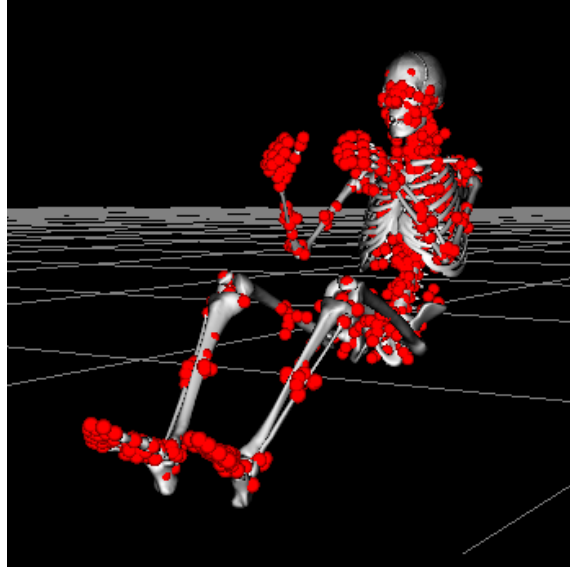


Figure 1. The center of mass location (red dots) of all FEM objects in the occupant version of the THUMS 50 percentile male are drawn with respect to the extracted skeleton structure.

2.2 Modeling the Actuation

The model is driven by three different actuator models. The arms are each equipped with 29 line-type muscle models (including bi-articular ones) [11]. They are simplified Hill-type muscle models consisting of a contractile (*CC*) and a parallel elastic element (*PE*), which is modeled as a linear elastic spring. The muscle force f^M is calculated as follows:

$$f^M = f^{PC} + f^{PE} = \alpha F_{max}^M f_l^M(l) f_v^M(v) + k(l - l_0^M), \quad (6)$$

with $\alpha \in [0, 1]$ the muscle activation level, F_{max}^M the maximum isometric muscle force, $f_l^M \in [0, 1]$ a length dependent force multiplier, $f_v^M \in \mathbb{R}$, a velocity dependent force multiplier, $k \in \mathbb{R}_0^+$ the spring stiffness of the *PE* element, and $l_0^M \in \mathbb{R}^+$ the optimal length of the muscle. The current length and contraction or lengthening velocity of the muscle is given by l and v , respectively. These muscle models were adapted to the kinematic properties of the THUMS model, taking into account the arm segment lengths. They move the shoulder, elbow, and wrist joint and perform upper arm flexion, extension, abduction, adduction, internal and external rotation, elbow flexion and extension, forearm pronation and supination, wrist flexion and extension and ulnar and radial deviation. For more information on this type of muscle model, see [11].

Eight muscle torque generators (MTG) [8] perform torso, hip, knee, and ankle flexion and extension. An MTG reflects the muscular properties for the deflection of one DoF in one direction. It has a similar position- and velocity-force dependence like the muscle models, only that in this case, everything is specified on joint level. The joint torque τ^{MTG} an MTG generates is derived as follows:

$$\tau^{MTG} = \tau_{max}^{MTG} \left(\alpha f_a^{MTG}(\theta) f_v^{MTG}(\omega) + f_p^{MTG}(\theta) \left(1 - \beta_p^{MTG} \frac{\omega}{\omega_{max}^{MTG}} \right) \right), \quad (7)$$

with τ_{max}^{MTG} the maximum isometric torque of the MTG, $\alpha \in [0, 1]$ the MTG activation, f_a^{MTG} , f_v^{MTG} , and f_p^{MTG} the joint angle dependent active torque multiplier, the velocity dependent torque multiplier, and the joint angle dependent passive torque multiplier, respectively. The passive torque multiplier is modeled as a exponential curve. To reduce oscillations, a damping term is included

with damping factor $\beta_p^{MTG} \in \mathbb{R}^+$, which depends on the joint velocity ω and the maximum joint angle velocity ω_{max}^{MTG} . The joint angle is denoted by θ . The parameters of the MTG are based on the MTG available in the open-source library RBDL [12], which were derived from experimental data available in the literature. For more information on this type of MTG, see [8] [12].

The remaining joints, for which no MTG or muscle model were available, are driven by simple torque sources,

$$\tau^{Motor} = \alpha \tau_{max}^{Motor}, \quad (8)$$

with $\alpha \in [0, 1]$ the activation level of the motor and τ_{max}^{Motor} the maximum torque the motor can produce. Similar to the MTG, 2 motors actuate 1 DoF of a joint.

2.3 Contact Modeling

The passenger interacts with the environment by standing on the bus floor and holding onto the handrail. This is modeled in the simulation over different contact constraint formulations. The hand and handrail is rigidly coupled at a single location defined by the initial position of the manikin,

$$\mathbf{g}_{hand}(\mathbf{q}) - \mathbf{g}_{hand}(\mathbf{q}_0) = \mathbf{0}, \quad (9)$$

with $\mathbf{g}_{hand} : \mathbb{R}^{n_{DoF}} \rightarrow \mathbb{R}^6$ calculating the position and orientation of the right palm with respect to the inertial frame based on given joint positions $\mathbf{q} \in \mathbb{R}^{n_{DoF}}$, and $\mathbf{q}_0 \in \mathbb{R}^{n_{DoF}}$ the joint positions at the beginning of the simulation. No limits on the contact forces and moments were specified in the simulation.

The contact between the feet and the bus floor is defined with respect to three points spanning a triangle. The three points are located at the heel P^{Heel} and the inner P^{IB} and outer P^{OB} side of the foot ball. The feet are placed on the ground according to the initial position \mathbf{q}_0 that specifies a light outward rotation of each foot by 5° with the foot sole parallel to the floor,

$$\mathbf{g}_{P^{Heel}}(\mathbf{q}) - \mathbf{g}_{P^{Heel}}(\mathbf{q}_0) = \mathbf{0}, \quad (10)$$

$$(\mathbf{g}_{P^{IB}}(\mathbf{q}) - \mathbf{g}_{P^{IB}}(\mathbf{q}_0))|_{y,z} = \mathbf{0}, \quad (11)$$

$$(\mathbf{g}_{P^{OB}}(\mathbf{q}) - \mathbf{g}_{P^{OB}}(\mathbf{q}_0))|_z = \mathbf{0}, \quad (12)$$

with $\mathbf{g}_P : \mathbb{R}^{n_{DoF}} \rightarrow \mathbb{R}^3$ calculating the position of point P with respect to the inertial frame. The position restricted to certain axes k is indicated by $|_k$. The contacts are modeled as sticking contacts, i.e., the normal contact forces f_N^P are to be non-negative and the tangential forces f_T^P are to remain within the friction cone defined by the normal contact forces.

$$f_N^P \geq 0, \quad P \in \{P^{Heel}, P^{IB}, P^{OB}\}, \quad (13)$$

$$|f_T^P| \leq k f_N^P, \quad P \in \{P^{Heel}, P^{IB}, P^{OB}\}, \quad (14)$$

$$(15)$$

with friction coefficient k set to 0.8 for the contact between shoe sole and floor.

2.4 Formulating the Bus Driveaway as Multi-Phase Optimal Control Problem

For simulating the passenger's behavior in a departing bus, two OCPs were set up and solved using the method of [11], which applies DMOCC [13]. The first OCP generated the initial position and

actuation of the manikin for the main OCP, which has following structure:

$$\min_{\mathbf{q}, \dot{\mathbf{q}}, \mathbf{u}} \mathbf{J}[\mathbf{q}, \dot{\mathbf{q}}, \mathbf{u}] = \sum_{i=0}^2 \int_{t_i}^{t_{i+1}} \Phi_i(\mathbf{q}, \dot{\mathbf{q}}, \mathbf{u}) dt \quad (16)$$

$$s.t. \quad \frac{\partial \mathbf{L}}{\partial \mathbf{q}}(\mathbf{q}, \dot{\mathbf{q}}) - \frac{d}{dt} \frac{\partial \mathbf{L}}{\partial \dot{\mathbf{q}}}(\mathbf{q}, \dot{\mathbf{q}}) + \mathbf{f}(\mathbf{q}, \dot{\mathbf{q}}, \mathbf{u}) + \mathbf{G}_i^T(\mathbf{q}) \boldsymbol{\lambda} = \mathbf{0}, \quad (17)$$

$$\mathbf{g}_i(\mathbf{q}) = \mathbf{0}, \quad (18)$$

$$\mathbf{h}_i(\mathbf{q}, \dot{\mathbf{q}}, \mathbf{u}) \geq \mathbf{0}, \quad i = 0, 1, 2, \quad (19)$$

with \mathbf{q} and $\dot{\mathbf{q}}$ the position and velocity of the system, respectively. The activation of the actuation of the system is denoted by \mathbf{u} , which are also the controls of the OCP. The objective Φ describes the behavior of the passenger. The constrained Euler-Lagrange equation of the system is given by Eq. (17) with \mathbf{f} the generalized forces, $\mathbf{G} = \frac{\partial \mathbf{g}}{\partial \mathbf{q}}$ the constraint Jacobian, and $\boldsymbol{\lambda}$ unknown force variables. The equality constraints include the contact constraints on positional level (9) and (10) - (12). Bounds on the variables and controls, constraints on the contact forces (13) and (14) and on the derivative of the controls are summarized in (19). The constraints on the derivative of the controls, the activation of the actuators, approximate the activation dynamics proposed by [14] using constant (de-)activation time constants T_d and T_a ,

$$-\frac{u_i}{T_d} \leq \dot{u}_i \leq \frac{1-u_i}{T_a}, \quad i = 1, \dots, N_a, \quad (20)$$

with N_a the number of actuators included in the human model. By applying these constraints, we avoid changes from no activation to full activation in a single time step of the control grid and limit the change in actuator activation to the physical capabilities of a human.

2.4.1 Organization of the Motion in Phases

The phases of the OCP are as follows (Fig. 2 right): At the beginning of the first phase, the bus starts moving. The passenger has a certain response time until it recognizes the changed conditions and reacts to them. To simulate this, the actuation of the manikin cannot change during this phase. During the second phase, the manikin is allowed to react to the accelerations. The phase ends when the desired target speed of the bus is reached. In the third and final phase, the manikin should return to a stable position within 1 second. Two different scenarios were considered: The passenger is oriented in driving direction and the passenger is standing with the back to the driving direction.

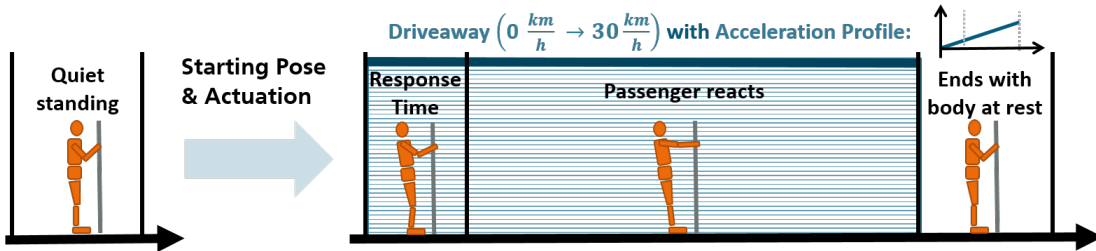


Figure 2. The simulation is organized in two OCPs. One calculates the starting position and actuation of the manikin (left) for the second OCP, which simulates the balance motion during the driveaway (right).

2.5 OCP for Start Position and Actuation

A second OCP (Fig. 2 left) was set up to compute a steady stance under various constraints on the posture. They are specified according to a common standing position of a passenger that holds onto a handrail: The elbow of the arm holding onto the handrail is flexed by 90° . The contact of the right hand with the vertical is be at shoulder level. The orientation of the right hand is within reasonable limits. The left arm is in a neutral position with slightly flexed elbow. For this purpose, the arm position of the pedestrian version of the THUMS model was adopted. The feet are parallel to the floor with a light outward rotation of 5° . The pelvis, torso, and head are upright, and the knees are straight. The calculated joint positions and actuation were adopted as starting condition in the OCP for simulating the bus driveaway.

2.5.1 Investigated Objective Functions

Two different objective functions were investigated for the driveaway simulation. Each objective function was applied in both scenarios. The first one, Φ^{AM} ,

$$\Phi^{AM} := c_M \|\mathbf{m}_{CoM}\|^2 + \boldsymbol{\alpha}^T \mathbf{W}_\alpha \boldsymbol{\alpha} + \dot{\boldsymbol{\alpha}}^T \mathbf{W}_{\dot{\alpha}} \dot{\boldsymbol{\alpha}} + \sum_{b \in B} c_b^\omega \|\boldsymbol{\omega}_b\|^2 + c_f \|\mathbf{f}_M^P\|^2 + c_\tau \|\boldsymbol{\tau}_{MTG}^P\|^2, \quad (21)$$

reduces a weighted combination of

- The activation $\boldsymbol{\alpha}$ of the human actuation weighted by diagonal matrix \mathbf{W}_α , since the human would choose an efficient motion.
- The derivative of the human actuation activation $\dot{\boldsymbol{\alpha}}$ weighted by diagonal matrix $\mathbf{W}_{\dot{\alpha}}$ to avoid large changes in the actuation.
- The angular momentum about the center of mass \mathbf{m}_{CoM} scaled by c_M , which is a common stability criteria.
- The angular velocity $\boldsymbol{\omega}_b$ with respect to the inertial frame scaled by c_b^ω of certain bodies b specified in the set B consisting of pelvis, torso, and head because the passenger would avoid sudden tilting of them and would want to keep is head facing forward.
- The passive muscle forces \mathbf{f}_M^P scaled by c_f and the passive MTG torques $\boldsymbol{\tau}_{MTG}^P$ scaled by c_τ to avoid exploitation of them.

The second one, Φ^{q_0} ,

$$\Phi^{q_0} := (\mathbf{q} - \mathbf{q}_0)^T \mathbf{W}_q (\mathbf{q} - \mathbf{q}_0) + \boldsymbol{\alpha}^T \mathbf{W}_\alpha \boldsymbol{\alpha} + \dot{\boldsymbol{\alpha}}^T \mathbf{W}_{\dot{\alpha}} \dot{\boldsymbol{\alpha}} + c_b^\omega \|\boldsymbol{\omega}_b^{Head}\|^2 + c_f \|\mathbf{f}_M^P\|^2 + c_\tau \|\boldsymbol{\tau}_{MTG}^P\|^2, \quad (22)$$

replaces the term on the angular momentum of the CoM and the angular velocity of the pelvis and torso by a term that enforces the manikin to remain in the initial position. The head was excluded (corresponding entries in the diagonal weighing matrix \mathbf{W}_q were set to 0), since we assumed that the passenger want to keep his head facing forward. Therefore, the term on the angular momentum of the head remained as well.

3 Results

The simulation was performed with two different stance configurations of the manikin, one oriented in the direction of driving (I) and the other opposite to the direction of driving (O). And two different objective functions were applied, Φ^{AM} that, among others, minimizes angular momentum of the center of mass (further denoted by AM), and Φ^{q_0} that, among others, minimizes the deviation to the initial position (further denoted by Q). For all cases, a linearly increasing acceleration

profile (jerk: 0.3 g/s) was applied until the platform reached a velocity of 30 km/h (see Figure 4 left).

The results with objective function AM resulted in significantly more dynamic motions (Figure 3). Impulsive motions were performed with the free arm and dynamic torso rotations were used to absorb the accelerations. In O + Q, by far the most arm force was required for the manikin to maintain its initial position while counteracting the accelerations (3.8 times as much as in O + AM, 2.2 times as much as in I + AM, and 1.8 times as much as in I + Q). The activation of motors and MTG was also highest in O + Q (1.1 times as much as in O + AM, 1.4 times as much as in I + AM, and 1.3 times as much as in I + Q). The maximum muscle activation that occurred in the arms during the simulation was 31% for O + AM, 100% for multiple muscles in the case of O + Q, 47% for I + AM, and 84% for I + Q.

In contrast, hand forces were lowest for O + Q (avg 80 N max. 125 N), followed by O + AM (avg 85 N max. 200 N), I + Q (avg 87 N max. 162 N), and I + AM (avg 95 N max. 168 N). The highest hand forces occurred for O + AM when the manikin pushes himself backward impulsively shortly after the response time (Figure 4 left). In the other cases, such an impulsive push was not optimized instead the hand forces gradually increased further after an initial sudden increase.

Looking at the distance between the combined center of pressure (CoP) of both feet and the nearest edge of the base of support (BoS), which is determined by the convex hull of the contact points between the feet and the floor, it can be observed that for both scenarios of O the boundary of the BoS is reached (Figure 4 right). For O + Q, the CoP is at the boundary of the BoS throughout the acceleration of the bus starting from the end of the response phase, while for O + AM, the distance between the CoP and the BoS recovers rapidly and assumes the highest values during the acceleration phase for all scenarios. For the two scenarios of I, the distance between CoP and BoS also decreases significantly after the response phase, but remains above 0. At the end of the motion, the distance is similar for all scenarios except for I + AM.

4 Discussion

The results show that in the case of O, the difference in actuation between AM and Q is much more significant than in the case of I. The manikin must exert significantly more energy and reaches its limit in arm muscle actuation for several muscles. The movement variant for O generated by AM, shows that an impulsive push backward is significantly more energy efficient. For the other scenario (I), although Q also requires significantly higher muscle actuation, the overall effort is not that different from (AM). In summary, scenario O is significantly more difficult for the manikin than I. Either more energy is required or higher dynamic movements are required to counteract the accelerations.

This methodology is well suited for analyzing the behavior of passengers in public transport and can be used to investigate many different scenarios. The application of the acceleration profiles is variable and can be replaced by more complex profiles than the ones shown here. Different behaviors can be modeled and investigated by changing the objective function. The influence of different standing poses can be investigated by replacing the starting posture, e.g. changing the locations of the contact between hand and handrail or the foot placement on the ground.

The contact models can still be improved. At the moment, the hand and the handrail are rigidly coupled. Limit values for the contact forces were not set in these simulations but could be added straightforwardly. However, a person must first build up tension before he or she can develop his or her full grasping force. A contact model that reflects this force buildup would make the simulations even more realistic. The foot was currently modeled as a sticking contact, where the foot always remains parallel to the ground. A standing passenger may lift the heel or foot ball to regain balance more quickly by shifting the center of gravity. A contact model as in [15] could model this behavior and improve further the simulation results.

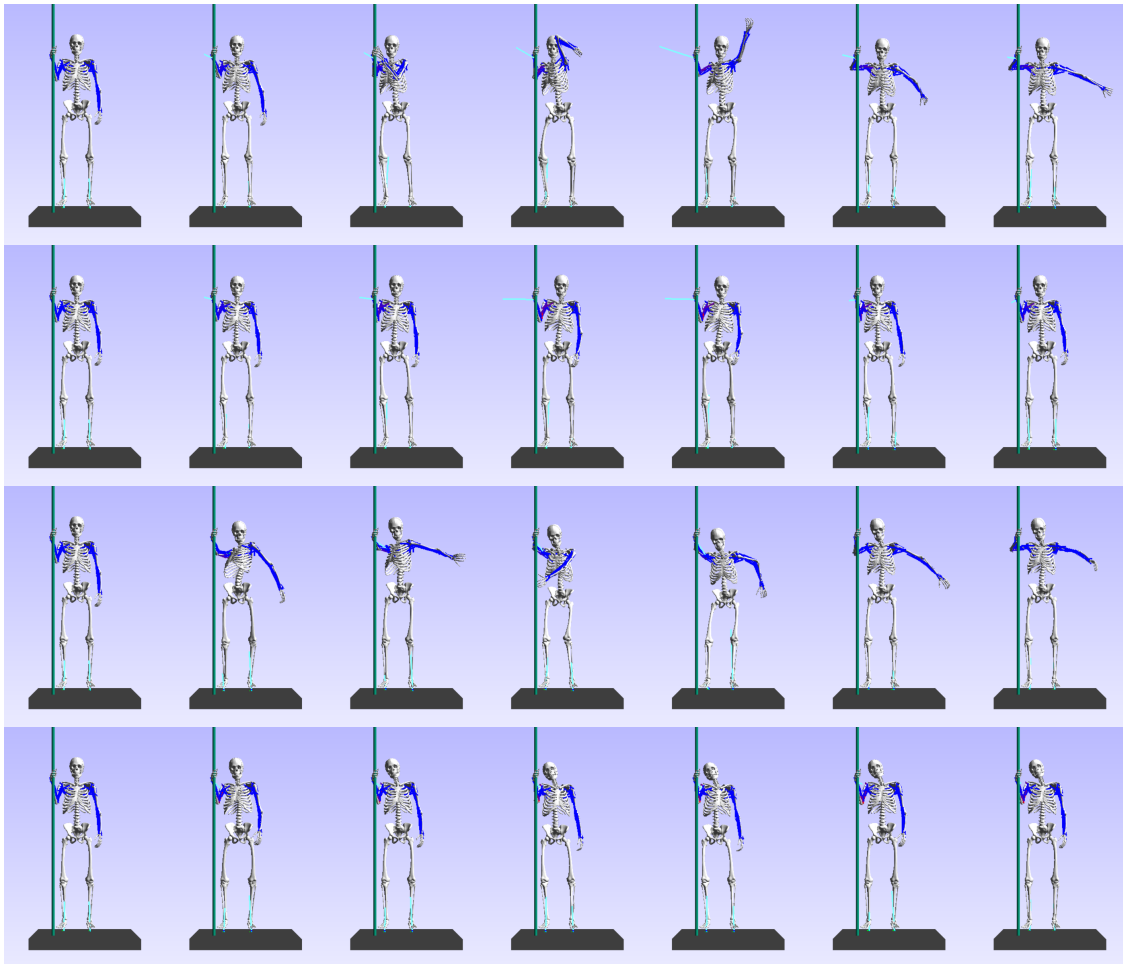


Figure 3. Snapshots of the simulated motions. Each row shows one motion. The camera perspective is moving with the platform. The contact forces are visualized by the light blue lines. The dark blue (not activated) to red (fully activated) lines at the arms represent the line-type muscle models. From top to bottom: I + AM, I + Q, O + AM, and O + Q.

5 Conclusion

We simulated the behavior of a standing passenger in a bus during driveaway using optimal control. The effects of two standing variants and two movement strategies on the optimized movement were investigated. It was shown that an orientation in the direction of travel is advantageous during the driveaway of the bus in order to compensate for the accelerations. The higher effort that would be required for an orientation against the driving direction can be significantly reduced by using highly dynamic movements. The knowledge gained in such simulations can be used as guidelines for the driving behavior of bus or train drivers and vehicle assistance systems to make public transport safer and more comfortable. In future work, we plan to validate our simulation results against experimental data.

ACKNOWLEDGMENTS

This work was supported within the Fraunhofer and DFG transfer programme.

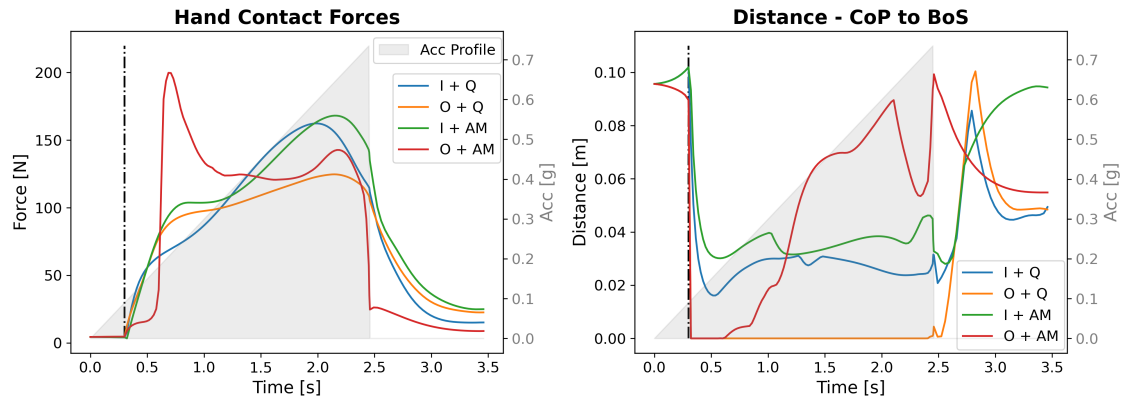


Figure 4. Left: Hand contact forces for the different scenarios. The acceleration profiles is plotted as grey area behind the curves. The black dashed line indicates the end of the response phase. **Right:** The minimal distance of the combined (left and right foot) center of pressure (CoP) to the boundary of the base of support (BoS) spanned by the contact points.

REFERENCES

- [1] Tran, T.D., Holtz, J., Müller, G., Müller, S.: Validation of madymo human body model in braking maneuver with highly reclined seatback. *International Journal of Crashworthiness* **27**(6) (2022) 1743–1752
- [2] Ambrosio, J., Carvalho, M., Milho, J., Escalante, S., Martin, R.: A validated railway vehicle interior layout with multibody dummies and finite element seats models for crash analysis. *Multibody System Dynamics* **54**(2) (2022) 179–212
- [3] Nie, H., Hu, M., Yin, F.: Ergonomics analysis of bus seat based on jack. In: 2021 IEEE 12th International Conference on Software Engineering and Service Science (ICSESS), IEEE (2021) 266–269
- [4] Iwamoto, M., Nakahira, Y., Tamura, A., Kimpara, H., Watanabe, I., Miki, K.: Development of advanced human models in thums. In: Proc. 6th European LS-DYNA Users' Conference. (2007) 47–56
- [5] Hu, J., Zhang, K., Reed, M.P., Wang, J.T., Neal, M., Lin, C.H.: Frontal crash simulations using parametric human models representing a diverse population. *Traffic injury prevention* **20**(sup1) (2019) S97–S105
- [6] van der Meulen, P., Seidl, A.: Ramsis—the leading cad tool for ergonomic analysis of vehicles. In: Digital Human Modeling: First International Conference on Digital Human Modeling, ICDHM 2007, Held as Part of HCI International 2007, Beijing, China, July 22-27, 2007. Proceedings 1, Springer (2007) 1008–1017
- [7] Inkol, K.A., Brown, C., McNally, W., Jansen, C., McPhee, J.: Muscle torque generators in multibody dynamic simulations of optimal sports performance. *Multibody System Dynamics* **50** (2020) 435–452
- [8] Millard, M., Emonds, A.L., Harant, M., Mombaur, K.: A reduced muscle model and planar musculoskeletal model fit for the simulation of whole-body movements. *Journal of biomechanics* **89** (2019) 11–20

- [9] Emonds, A.L., Funken, J., Potthast, W., Mombaur, K.: Comparison of sprinting with and without running-specific prostheses using optimal control techniques. *Robotica* **37**(12) (2019) 2176–2194
- [10] Beillas, P., Wang, X., Lafon, Y., Frechede, B., Janak, T., Dupeux, T., Mear, M., Pacquaut, G., Chevalier, M.C., Le Ruyet, A., Eichene, A., Theodorakos, I., Yin, X., Gardegaront, M., Collot, J., Petit, P., Song, E., Moreau, B., Kleiven, S., Giordano, C., Strömbäck Alvarez, V., Li, X., Kirscht, S., Saeed, A., Goede, W., Holtz, J., Chawla, A., Chhabra, A., Paruchuri, S., Singh, S., Kaushik, D., Mukherjee, S., Kumar, S., Devane, K., Mishra, K., Machina, G., Jolivet, E., Potier, P., Potier, C., Loury, D., Baudrit, P., Faure, F., Lemaire, T., Gilles, B., Vimont, U., Praxl, N., Peres, J., Bhaskar, A., Lecomte, C., Bah, M., Odet, P.: PIPER EU Project Final publishable summary. Research report, IFSTTAR - Institut Français des Sciences et Technologies des Transports, de l'Aménagement et des Réseaux (January 2017)
- [11] Roller, M., Björkenstam, S., Linn, J., Leyendecker, S.: Optimal control of a biomechanical multibody model for the dynamic simulation of working tasks. In: 8th ECCOMAS Thematic Conference on Multibody Dynamics, Prague, Czech Republic (June 2017)
- [12] Felis, M.L.: RBDL: An efficient rigid-body dynamics library using recursive algorithms. *Autonomous Robots* (2016) 1–17
- [13] Leyendecker, S., Blöbaum, S., Marsden, J., Ortiz, M.: Discrete mechanics and optimal control for constrained systems. *Optimal control applications & methods* **31**(6) (2010) 505–528
- [14] Winters, J.M.: An improved muscle-reflex actuator for use in large-scale neuromusculoskeletal models. *Annals of Biomedical Engineering* **23**(4) (Jul 1995) 359–374
- [15] Millard, M., Mombaur, K.: A quick turn of foot: Rigid foot-ground contact models for human motion prediction. *Frontiers in Neurobotics* **13** (2019)